Available online at www.sciencedirect.com
SCIENCE DIRECT
Polymer 47 (2006) 5420–5428
polymer
www.elsevier.com/locate/polymer

Microphase separation and crystallization in mixtures of polystyrene–poly (methyl methacrylate) diblock copolymer and poly(vinylidene fluoride)

Jong Kwan Lee [a], Ji Seon Kim [a], Hae Jin Lim [a], Kwang Hee Lee [a,*], Seong Mo Jo [b], Toshiaki Ougizawa [c]

[a] *Department of Polymer Science and Engineering, Inha University, 253, Yonghyun-dong, Nam-gu, Incheon 402-751, South Korea*
[b] *Polymer Hybrids Research Center, Korea Institute of Science and Technology, Seoul 136-791, South Korea*
[c] *Graduate School of Science and Engineering, Tokyo Institute of Technology, Tokyo 152-8550, Japan*

Received 18 October 2005; received in revised form 16 March 2006; accepted 4 May 2006
Available online 13 June 2006

Abstract

This study examined the microdomain structures and the crystallization behavior in binary blends consisting of an asymmetric block copolymer and a homopolymer using small-angle X-ray scattering, optical microscopy and differential scanning calorimetry. A polystyrene-block-poly(methyl methacrylate) copolymer (PS-*b*-PMMA) was mixed with a low molecular weight poly(vinylidene fluoride) (PVDF), where the PS-*b*-PMMA had a 0.30 wt fraction of the PMMA block. At a PVDF concentration of <13.0 wt%, the PVDF was completely miscible with the PMMA microdomains, and the blends had a cylindrical structure. The addition of PVDF altered the morphology from a PMMA-cylindrical structure to a lamellar structure and finally to a PS-cylindrical structure. When the PVDF concentration was <23.0 wt%, the PVDF was distributed uniformly within the PMMA microdomains. After adding more PVDF, some of the PVDF was locally dissolved in the middle of the PMMA microdomains. The addition of PVDF also affected the ordered microstructure in the blends, leading to a well-defined microdomain structure. However, PVDF crystallization significantly disturbed the pre-existing microdomain structure, resulting in a poorly ordered morphology. In the blends, PVDF had unique crystallization behavior as a result of the space constraints imposed by the microdomains.

Keywords: Block copolymer; Microphase separation; Crystallization

1. Introduction

In recent years, many studies have been carried out to determine the morphology of binary mixtures containing a block copolymer with a homopolymer [1–25]. The addition of a homopolymer to a block copolymer can cause changes in the microstructures and properties of the block copolymer. However, the choice of miscible homopolymers for mixing with block copolymers is limited on account of the poor miscibility of most polymer pairs. Most studies used homopolymers with repeat units identical to one of the blocks in the block copolymers [1–19]. Relatively, a few studies have considered blends where the homopolymer is different from either the segments of the block copolymer but is miscible with one of the blocks [20–25].

One important difference between a homopolymer/block copolymer blend and a homopolymer/homopolymer blend is that the homopolymer has limited solubility in the microdomains of a block copolymer. It is expected that the solubility of a homopolymer in the microdomains of a block copolymer will depend on the molecular weight ratio of the homopolymer and the appropriate block of the block copolymer (M_H/M_B), specific interactions between the homopolymer and the block copolymer, the microstructure geometry, and temperature. Various thermodynamic theories predict the solubility of a homopolymer in a block copolymer. Meier [6] reported that significant solubility of a homopolymer in a block copolymer occurs when $M_H/M_B<1$. The maximum solubility of homopolymer A in the A-phase of an AB or ABA block copolymer is estimated to be approximately 14 vol% if the block copolymer microstructure is lamellar and the $M_H/M_B=1$. However, it is possible to achieve a high solubility even when the M_H/M_B is >1 in a strong interaction system. Lei and Weiss [21] examined the phase behavior of the blends of a lightly sulfonated styrenic block copolymer and poly(caprolactone) (PCL). The blend had a lamellar microstructure and a

* Corresponding author. Tel.: +82 32 862 9507; fax: +82 32 865 5178.
E-mail address: polylee@inha.ac.kr (K.H. Lee).

0032-3861/$ - see front matter © 2006 Elsevier Ltd. All rights reserved.
doi:10.1016/j.polymer.2006.05.022

$M_H/M_B = 5.3$. They reported that the solubility limit within a sulfonated polystyrene block was approximately 46 wt% PCL, which is much higher than predicted theoretically. The enhanced solubility is believed to be the result of exothermic interactions between the sulfonic acid groups of the sulfonated polystyrene block and the ester groups of the PCL. They concluded that the solubility limit for a homopolymer/block copolymer blend increases with increasing strength of the specific interactions.

The differences between a homopolymer/block copolymer blend and a homopolymer/homopolymer blend can be also found in blends involving components that can crystallize [7–17,22]. For example, the crystallization of a homopolymer will be affected by blending it with an amorphous block copolymer. Both the block copolymer microstructure and the solubility of the homopolymer in the microdomains of a block copolymer should influence the crystallization behavior, which is likely to be different from that of a homopolymer/homopolymer blend or in a neat block copolymer with a block that can crystallize. There are three factors that determine the morphology and crystallization behavior of homopolymer/amorphous block copolymer blends, the microphase separation of a block copolymer (the order–disorder transition temperature, T_{ODT}), the crystallization of the homopolymer (the crystallization temperature, T_c), and the verification of amorphous blocks (the glass transition temperature, T_g). Competition between these three processes can be understood by the relative positions of the corresponding three temperatures. When $T_{ODT} < T_c$, unconfined crystallization occurs from a disordered phase, while crystallization takes place from an ordered phase when $T_{ODT} > T_c$. Crystallization becomes confined when $T_{ODT} > T_g > T_c$, and the existing phase morphology exerts strong restrictions on crystallization. Partially confined crystallization may also occur in some cases involving strongly segregated block copolymer systems, although $T_c > T_g$. This may be due to strong microphase separation between the two immiscible blocks.

This paper describes various blends of a amorphous diblock copolymer poly(methyl methacrylate)-block-polystyrene (PS-*b*-PMMA) with a semicrystalline homopolymer poly(vinylidene fluoride) (PVDF), which has a favorable interaction with one of the blocks, PMMA in this case [26–28]. This system was chosen to provide an insight into how the addition of a homopolymer affects the morphological change in a block copolymer. An additional aim of this study was to determine how a restricted geometry, i.e. the block copolymer domains, affects the crystallization behavior of PVDF. A complicated morphology was anticipated in this blended system because of microphase separation in the block copolymer and PVDF crystallization. Therefore, the phase morphology of each individual blend in the melt was first determined using small-angle X-ray scattering (SAXS). The microphase-separated and annealed melt was then cooled to a certain temperature, and the crystalline structures and the microphase morphology were investigated after subsequent crystallization. The crystallization kinetics and the melting behavior were investigated using differential scanning calorimetry (DSC).

2. Experimental

2.1. Materials

The asymmetric PS-*b*-PMMA with a polydispersity index $M_w/M_n = 1.04$ was obtained from the Polymer Nano-patterned Materials and Nano-rheology Laboratory of Pohang University (Korea). The M_n of the PMMA and PS blocks was 2.9×10^4 and 6.8×10^4, respectively. The previous studies [29–31] reported that the block copolymer showed the best hexagonal packing of the microdomains when annealed at 170–180 °C. The order–disorder transition for this material was not accessible since it might lie above the decomposition temperature. The low molecular weight PVDF ($M_n = 5.0 \times 10^3$) was obtained from the Polymer Hybrids Research Center of Korea Institute of Science and Technology. The synthesis and characterization of the PVDF are described elsewhere [32]. A series of PVDF and PS-*b*-PMMA blends were prepared using the solvent-casting method. Predetermined amounts of PVDF and PS-*b*-PMMA were dissolved in *N*,*N*-dimethylacetamide (DMAc) (ca. 10 wt% solution). The solvent was evaporated slowly over a one-week period at room temperature and dried under vacuum for 5 days at 60 °C. In order to confirm the miscibility, PVDF/PS/PMMA ternary blend with a composition of 23/54/23 (w/w/w) was also prepared via the same procedure. The residual solvent was removed and the formation of an ordered microphase structure was induced by annealing the cast films under vacuum for 3 days at 180 °C. The annealed samples were quickly quenched in liquid nitrogen to freeze the structure in the melt. The compositions of the blends are listed in Table 1.

2.2. DSC

Thermal analyses of the blends were carried out using a DSC 2920 (TA Instruments). The modulated DSC mode was used to measure the glass transition (T_g). The measurements were taken at temperatures ranging from −40 to 120 °C. The heating rate, oscillation amplitude and oscillation period were 2 °C/min, 1 °C and 60 s, respectively. The reversing heat flow curve was used to determine the T_gs. The DSC cooling thermograms were obtained by annealing the samples for 10 min at 180 °C and cooling them at a rate of −10 °C /min

Table 1
Composition of the PVDF/PS-*b*-PMMA blends

Nomenclature	$W_{(PVDF)}$ [a]	$W_{(PVDF+PMMA)}$ [b]
B1	0.07	0.35
B2	0.13	0.39
B3	0.18	0.43
B4	0.23	0.46
B5	0.31	0.52
B6	0.38	0.56
B7	0.55	0.68

[a] Weight fraction of PVDF.
[b] Weight fraction of PVDF and PMMA block of the copolymer.

from 180 to −40 °C. The melting thermograms were obtained by heating the samples at a rate of 10 °C/min.

2.3. Optical microscopy

The miscibility in the melt state and the crystalline morphology of the blends were examined using a Nikon Optiphot 2 microscope equipped with a hot stage. The blends were first melted at 180 °C for 10 min, and isothermally crystallized at the crystallization temperature $T_c = 135$ °C. Micrographs of the crystallized samples were taken between crossed polarizers.

2.4. SAXS

The SAXS experiments were conducted at the synchrotron X-ray beam line 4C1 of the Pohang Light Source (PLS), Korea [33]. The wavelength of the X-ray beam was 0.1608 nm. The distance between the detector and the sample was 170 cm. The scattering intensity (I) was corrected for background scattering. The scattering intensity as a result of the thermal fluctuations was then subtracted from the SAXS profile $I(q)$ by evaluating the slope of a $I(q)q^4$ versus q^4 plot at the wide scattering vector q, where q is $(4\pi/\lambda)\sin(\theta/2)$, with λ and θ being the wavelength and scattering angle, respectively. A correction for the smearing effect due to the finite cross-section of the incident beam was not necessary for the optics of the SAXS with point focusing.

2.5. Transmission electron microscopy (TEM)

The microphase morphology of the blends was investigated by cross-sectional TEM. The blend films were first embedded with epoxy resin. After curing the epoxy resin at room temperature for 12 h, thin sections (ca. 70 mm thick) were obtained using a Reichert Ultra Microtome with a diamond knife. The sectioned samples were exposed to RuO_4 (0.5% aqueous solution) for about 10 min to stain the PS block selectively. TEM was performed on a JEOL 1200EX operating at 120 kV.

3. Results and discussion

3.1. Morphology

Fig. 1 shows the optical micrographs of the melt morphology of the 23/77 (w/w) PVDF/PS-*b*-PMMA blend (B4) and the 23/54/23 (w/w/w) PVDF/PS/PMMA ternary blend with the same composition of B4. The PVDF/PS-*b*-PMMA blend shows a single phase while the PVDF/PS/PMMA blend shows a macrophase-separated structure that is typical of an immiscible blend system. Macro-phase separation in the PVDF/PS/PMMA blend was expected because PS is immiscible with either PMMA or PVDF. However, the appearance of a single phase in the wide range of compositions between B1 and B7 (The optical micrographs were omitted) is quite interesting considering the fact that the homopolymer has

Fig. 1. Optical micrographs of the blends at 180 °C (a)PVDF/PS-*b*-PMMA 77/27 (w/w) and (b) PVDF/PS/PMMA 23/54/23 (w/w/w).

limited solubility in the microdomains of the block copolymer [4,12,21]. Such a large solubility may be attributed to the relatively small molecular weight of PVDF compared with that of the PMMA block. The strong interaction between the PVDF and PMMA block should also contribute to form a single-phase morphology.

The possible states of the PVDF incorporated into the PMMA-block domain without any macro-separation are as follows: (1) PVDF is dissolved in the PMMA microdomain; (2) some PVDF is dissolved in the PMMA microdomain, while some PVDF is restricted to the center of the microdomain; (3) PVDF is located within the PMMA microdomain, but the PVDF is completely segregated from the PMMA segment, resulting in the formation of a phase-separated structure that is similar to a core-shell structure. This study examined how the PVDF exists in the PMMA microdomain by measuring the T_gs of the blends. Fig. 2 shows the change in the T_g as a fraction of the blend composition. The PS-*b*-PMMA has a single T_g because the T_gs of the two components of the block copolymer are similar. On the other hand, the blends show two T_gs, which

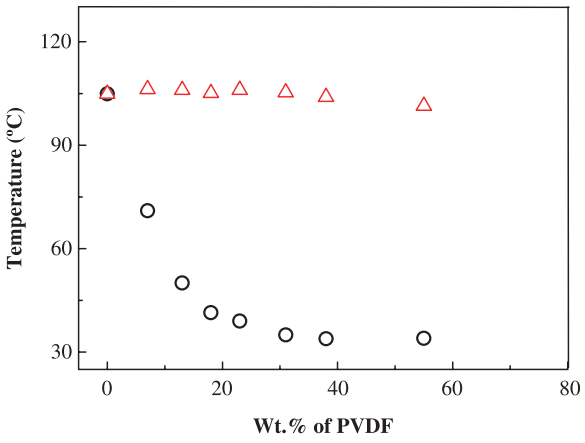

Fig. 2. Glass transition temperatures of the PVDF/PS-*b*-PMMA blends.

was attributed to a change in the T_g of the PMMA microdomain due to the incorporation of PVDF. It should be noted that the T_g of the PS microdomain is almost constant, irrespective of the blend composition, indicating that the increase in the mobility of the PMMA segments due to the incorporation of PVDF has no effect on the mobility of the PS segments. This suggests that the PMMA and PS segments of the block copolymer are highly segregated and the block copolymer has a sharp interface. One of important features in Fig. 2 is the T_g behavior of the PMMA microdomains. The T_g of the PMMA microdomain decreases with increasing PVDF concentration up to ca. 30 wt%, and is constant thereafter. The following conclusions can be made when considering the theoretical change in the T_g based on the miscibility of PMMA and PVDF at all compositions. At a low PVDF concentration such as B1 and B2, the PVDF is well mixed with the PMMA segments at the molecular level. As the PVDF concentration is increased, some PVDF is not dissolved, and becomes confined to a small area at the center of the PMMA microdomain. If the PVDF content in the blend increases above B5, the PVDF solubility of the PMMA microdomain reaches a limit, i.e. saturation. Therefore, further PVDF addition only increases the dimensions of the PVDF core and does not affect the T_g of the PMMA microdomain (the dimensional change in the microdomain will be discussed in Section 3.1). In this study, there was no T_g of the PVDF core. This can be attributed to the following: (1) DSC has a limited resolution; and (2) the core PVDF can be crystallized even if the sample is quenched (crystallization of the core PVDF will be discussed in Section 3.2). As a result, the T_g of the amorphous PVDF could not be detected.

A block copolymer consisting of mutually immiscible polymers forms microdomain structures such as alternating lamellar, cylindrical, and spherical microdomains. In the strong segregation limit, the morphology depends on the volume fraction of one of the constituent block chains (f). There are many reports classifying the morphologies in terms of f [34]. The following sequence of phases is observed for the A-*b*-B diblock copolymer; $f_A < 0.25$, spherical microdomain; $0.25 < f_A < 0.4$, cylindrical microdomain; $0.4 < f_A < 0.5$, lamellar microdomain. The microstructure of the block copolymer can be determined using small-angle X-ray scattering (SAXS), small-angle neutron scattering (SANS) and transmission electron microscopy (TEM). In this study, the microphase morphology of the block copolymer and its blends in the molten state was determined from the scattering peak positions in SAXS pattern. Fig. 3 shows the SAXS patterns at different blend compositions. The block copolymer (B0) exhibits multiple-order scattering maxima at the peak positions (q_m) of $1:(3)^{1/2}:(7)^{1/2}$ relative to that of the first-order peak (q^*), where q is $(4\pi/\lambda)\sin(\theta/2)$, with λ and θ being the wavelength and scattering angle, respectively. The peak position ratio (q_m/q^*) suggests that the block copolymer has a hexagonally packed cylindrical microdomain structure [34]. The blend, B1, also shows a scattering pattern corresponding to a cylindrical microdomain structure, but had higher order peaks, which could not be observed in B0. The ordering of the microstructure of PS-*b*-PMMA according to the PVDF addition may be interpreted kinetically. Low molecular weight PVDF, which is in the molten state at the annealing temperature of 180 °C, acts as a plasticizer for the PMMA microdomains, which increases the mobility of the PMMA-segment. The enhanced mobility of the PMMA segments may assist the development of well-ordered microstructures. The blend morphology is changed with increasing PVDF content. For blends with a PVDF weight fraction ranging from 0.18 (B3) to 0.38 (B6), q_m/q^* in the scattering patterns was 1:2:3. This means that the blend morphology changes from a cylindrical microdomain structure to a lamellar microdomain structure. Indeed, the weight fraction of the PMMA phase including the PVDF fraction for B3 to B6 ranged from 0.43 to 0.56. Considering these fractions, it is expected that the microdomains of these blends will consist of lamellae. The intensity of the second-order scattering peak for the blends with a lamellar structure is weaker than that of the third-order scattering peak. This can be is understood based on the 'extinction rule of structural symmetry' [2]. The volume fractions of the PS and PMMA phases in the lamellar structure are close to 0.5, which result in a decrease in the intensity of the second-order scattering peak. The further addition of PVDF induces a change in morphology from a lamellar to a cylindrical structure. The blend with a 0.55 wt fraction of PVDF (B7) shows a scattering pattern with a q_m/q^* ratio of $1:(3)^{1/2}:(13)^{1/2}$, which corresponds to a cylindrical microdomain structure. Therefore, the addition of PVDF changes the blend morphology from a PMMA-cylindrical to a lamellar and finally to a PS-cylindrical structure.

The interdomain distance, D can be determined from the Bragg spacing calculated from the first-order scattering peak as follows: for an alternating lamellar structure, $D = d_{100}$; for a hexagonally packed cylindrical structure, $D = (4/3)^{1/2} d_{100}$ [7]. Fig. 4 shows the change in D as a function of the blend composition. When the PVDF fraction was < 0.13, the D value slightly decreases with increasing PVDF concentration. The decrease in the D values suggests that the interdomain distance might be reduced by the swelling of the PMMA cylindrical domain due to the incorporation of PVDF molecules. The abrupt change in D at a certain weight fraction of PMMA–PVDF phase (in the Figure, approximately 0.4 and 0.65) demonstrates that the transition of the microdomain structures

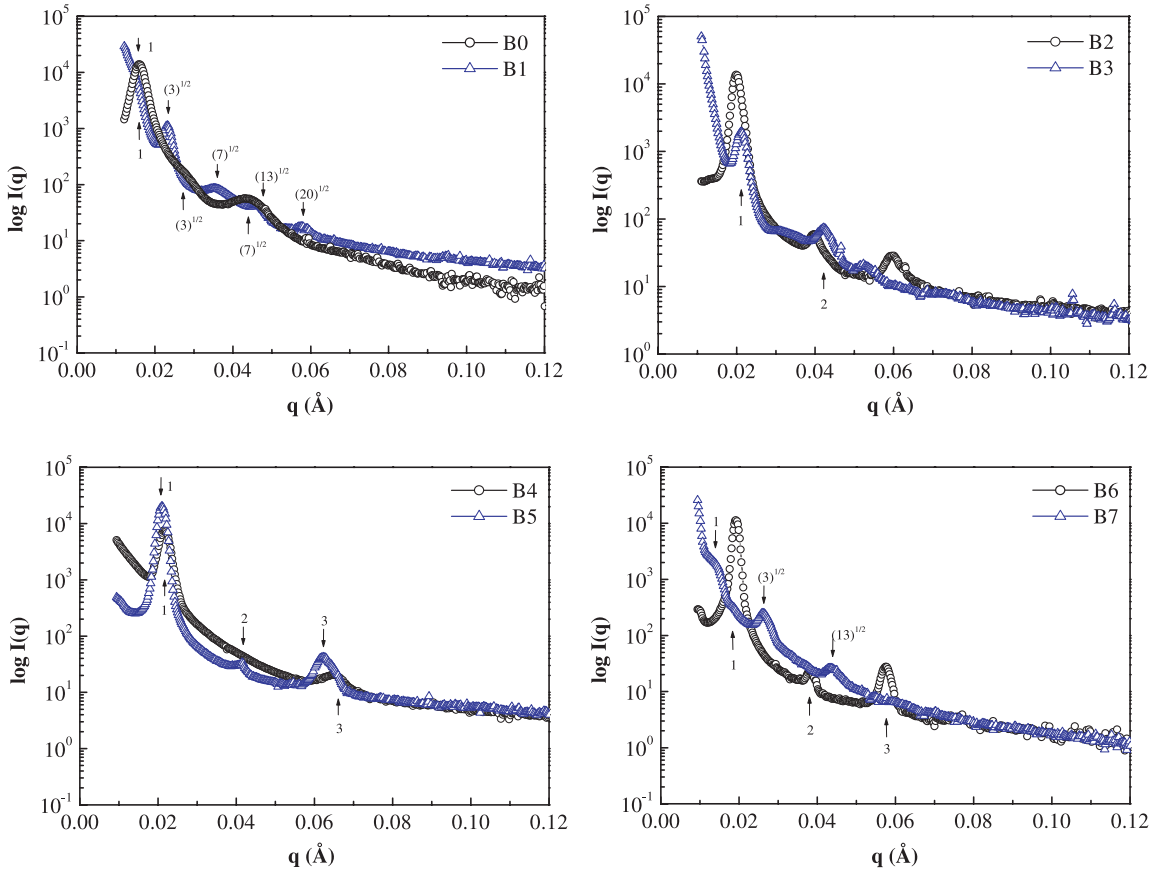

Fig. 3. SAXS profiles of the PS-*b*-PMMA and PVDF/PS-*b*-PMMA blends in the amorphous state.

of the block copolymer, PS-*b*-PMMA, occurs as a result of PVDF addition.

TEM provided additional evidence for the morphology transition (Fig. 5). The block copolymer (B0) and the blends with a small amount of PVDF (B1 and B2) shows well-developed cylindrical structures, as expected from the SAXS patterns. A morphology transition occurs with increasing the PVDF concentration. The lamellar morphology is observed for the B3–B6 blends. A microdomain structure cannot be found in case of B7, and only a fibrillar structure of PVDF crystals can be seen. In the molten state, B7 shows a distinct SAXS pattern corresponding to a cylindrical microdomain structure. Therefore, the TEM result suggests that the crystallization of PVDF influences the pre-existed microdomain structures.

In general, polymeric crystals grow at a long-range order of micrometer. Therefore, a subsequent crystallization process may disturb a pre-existing microdomain structure. In particular, it is possible that the micro-morphology may be significantly distorted if the crystallization temperature is higher than the T_g values of block segments. Fig. 6 shows the changes in the SAXS patterns before and after crystallization. In the case of B1, two SAXS profiles before and after crystallization show multiple scattering peaks corresponding to the cylindrical microdomain structure, and the peak positions are almost the same. This indicates that at low PVDF concentrations, PVDF crystallization may be restricted within the PMMA phase, having no influence on the pre-existing microdomain structure. The scattering profiles become broad with increasing PVDF concentration, implying that the domain structures are disturbed due to PVDF crystallization. During crystallization, the PVDF crystal front advances by locating and following the PMMA–PVDF phase in the microdomain structure. The PS and PMMA-block domains are in the rubbery phase at the crystallization temperature (135 °C). Therefore, it is likely that the crystal front grown at a long-range order will cause a rearrangement and/or disturbances in the microdomain structures. For blends with a higher PVDF concentration, where the PVDF core structure appears, the crystalline phase of

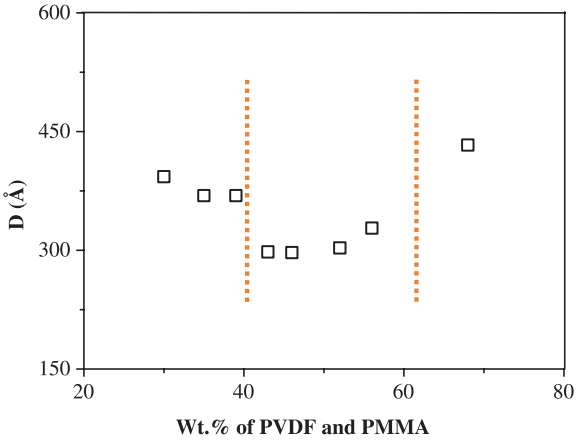

Fig. 4. Interdomain distance (*D*) as a function of the blend composition.

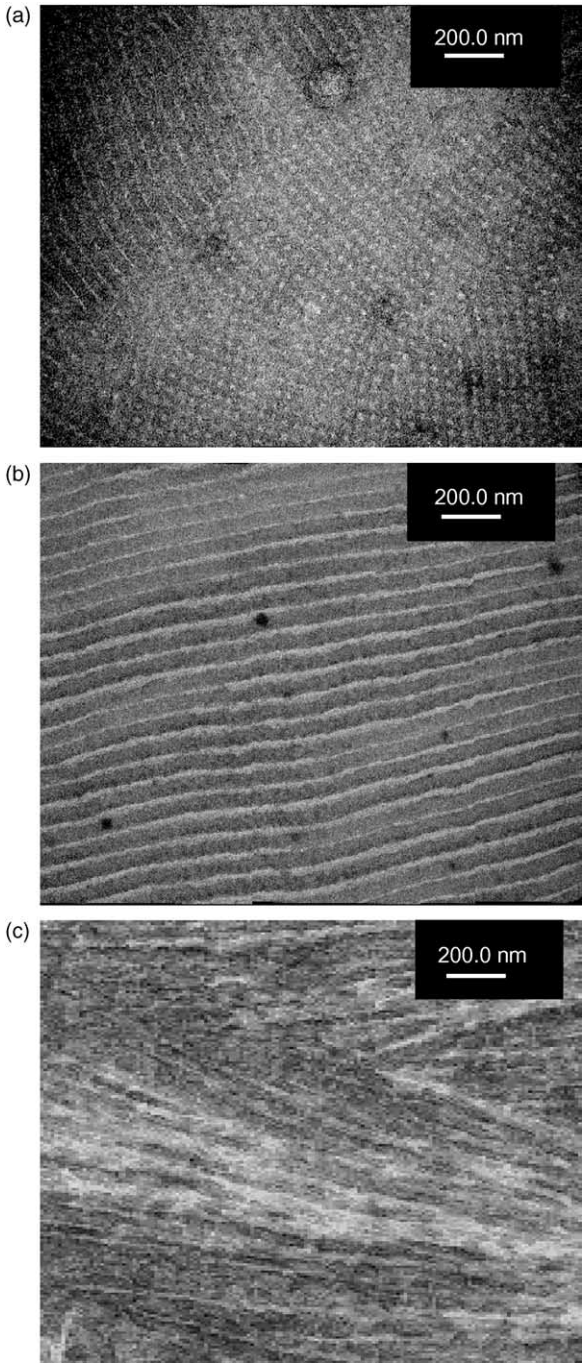

Fig. 5. TEM micrographs of the PVDF/PS-*b*-PMMA blends; (a) B1; (b) B5; (c) B7.

the core PVDF consists of a three-phase structure with PMMA and PS-block domains. The three-phase structure may perturb the long-range electron densities, resulting in a broadening of the SAXS profiles. One of interesting features in the Figure is the change in the long period, L of the PVDF crystals (the q value corresponding to L is denoted as an arrow in the Figure). The L value of B3 and B7 are 9.4, and 9.8 nm, respectively. These values are similar to the L value of 9.5 nm for the homo-PVDF (SAXS pattern for the homo-PVDF is not shown). This means that the lamellar thickness is almost independent of the pre-existing microdomain structures, even though the confined crystallization proceeds within the ordered-phase morphology. It is worth noting that there are many studies on the orientation of the emerging crystals within the microdomains. Cohen et al. [35,36] demonstrated, through X-ray pole figure analysis, that the chain axis of the crystals is perpendicular to the normal direction of the microphase-separated lamellar surfaces. Liu and Chu [37] studied the crystalline structure of poly(tetrahydrofuran) (PTHF) in blends of the diblock copolymer and homo PTHF and proposed a model in which the crystallized chains were parallel to the lamellar normals. Other researchers have also studied lamellar systems, using the shear forces for the alignment of the microphase-separated block copolymer structures, and found that the orientation of the chain axis of the crystals depends on several factors, such as the molecular weight of the block copolymer and the crystallization conditions [38-40]. Quiram et al. [41] used a channel die to study the crystal orientation in a sample, wherein the crystallizable block constituted the cylindrical microdomains, and demonstrated that the crystalline lamellae grow along the cylinder axis. Loo et al. [42] examined the solid-state structures of cylinder-forming semicrystalline diblock copolymers, wherein the crystals are compelled to remain outside of the cylinders. They found that the hexagonally packed cylindrical microdomains produce a preferential orientation, in two dimensions, of the crystals. Park et al. [43] also studied the orientation of the crystals formed between the cylinders and reported that the b and c axes of the crystals are predominantly parallel and perpendicular to the axes of the cylinders, respectively. It is clear that most of the previous studies on this issue have been made using small- and wide-angle X-ray scattering combined with TEM. With the present data, therefore, no definite conclusion can be reached. Further studies will be necessary to confirm the orientation of the crystals with respect to the microdomain interfaces.

3.2. Crystallization

The crystallization behavior of the blends appears to be significantly different from that of the homo-PVDF because the microdomain structure in the melt state provides spatial constraints to crystal growth. It is believed that the microdomain structures may impose nanoscale confinement to retard crystal growth [44,45]. There are two classifications of confined crystallization in an ordered phase morphology. The first is the crystallization temperature (T_c) < the glass transition temperature of the block segments (T_g) < the order–disorder transition temperature of the block copolymer (T_{ODT}). In that case, the crystallization of a homopolymer is strongly confined by the glassy blocks within the pre-existing phase morphology. This is known as hard confinement. The second case is where $T_g < T_c < T_{ODT}$, which is known as soft confinement. However, the ability of PVDF to crystallize under the conditions of hard confinement is too low to confirm any crystallinity or crystalline morphology using DSC and optical microscopy. Therefore, the crystallization in this work was performed under the condition of $T_g < T_c$.

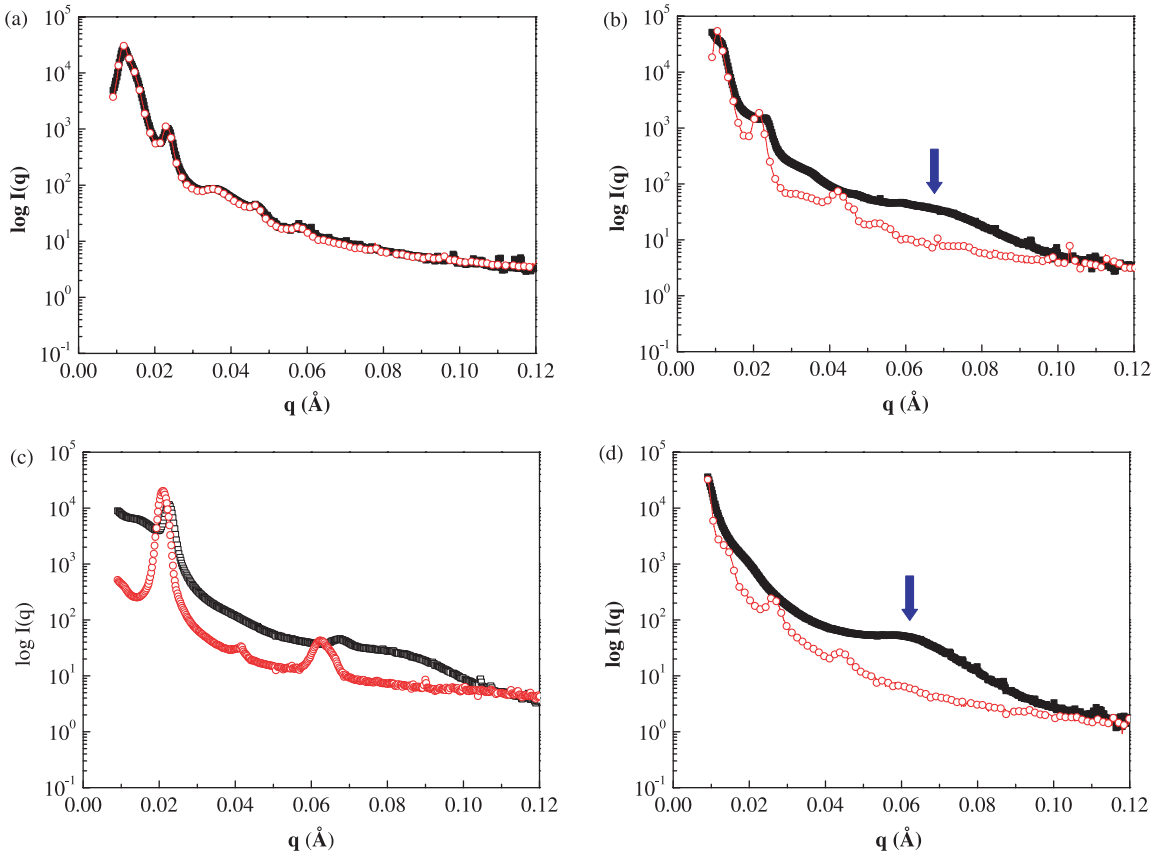

Fig. 6. SAXS profiles of the amorphous (○) and crystallized (●) PVDF/PS-*b*-PMMA blends; (a) B1; (b) B3; (c) B5; (d) B7.

Fig. 7 shows optical micrographs with crossed polarizers for the blend samples crystallized at 135 °C over a 5 day period after inducing the microdomain structure in the melt. No samples showed the spherulitic structure, which is similar in appearance to a 'Maltese Cross' extinction pattern. That means that the pre-existing microdomain structures restrict the lamellar orientations and favor the random arrangement of individual lamellar crystallites.

The effects of the confined crystallization on the melting behavior of PVDF were evaluated (Fig. 8). PVDF shows multiple melting endotherms after isothermal crystallization at 135 °C. PVDF has multiphase characteristics with four widely accepted crystalline forms (α, β, γ and δ also known as I, II, III and IV, respectively), [46]. The β-phase, with an almost planar zigzag conformation, has the highest piero-electric constant. The α-phase, although it has a TGTG′ conformation, is electrically inactive because the molecular dipoles in the unit cell negate each other. When considering that the melting temperatures of the α- and β-phase of the PVDF crystal forms are similar, such a multiple melting behavior may be associated with melting, recrystallization, and remelting in the melting region. One interesting feature is that higher melting endotherms can be observed for the blend samples. The melting temperature (T_m) can be expressed as a ratio of the change in the enthalpy (ΔH_m) and entropy (ΔS_m) during melting ($T_m = \Delta H_m/\Delta S_m$). ΔH_m is a term that is determined by the interaction between the molecular chains, and is almost

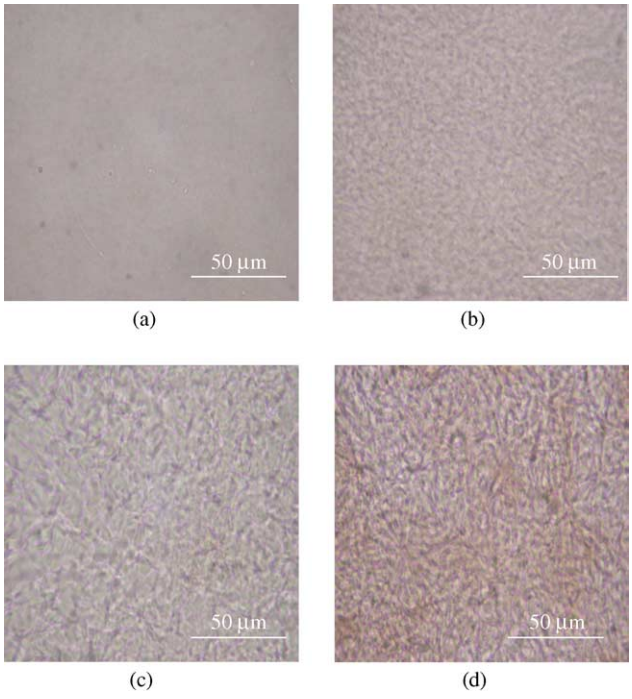

Fig. 7. Optical micrographs of the PVDF/PS-*b*-PMMA blends crystallized at 135 °C (a) B1; (b) B3; (c) B5; (d) B7.

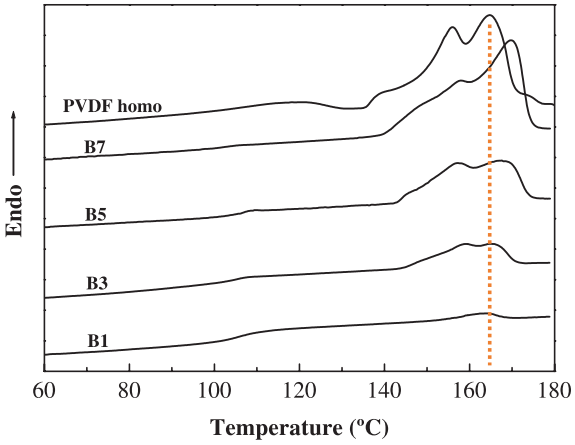

Fig. 8. Melting endotherms of the homo-PVDF and PVDF/PS-*b*-PMMA blends. The heating rate was 10 °C/min.

constant if the crystalline structure is similar. One the other hand, ΔS_m depends on the chain conformations of the melt and crystalline state, and is mainly controlled by the freedom of the chain conformation in the melt state. For the blends with a high PVDF content, some PVDF is localized at the center of the PMMA microdomains and is spatially confined at the nanoscale. The confined molecules have a relatively lower degree of freedom in the chain conformation than molecules in free space. As a result, the ΔS_m of the confined molecules is smaller than that of the free molecules. According to the formula, $T_m = \Delta H_m/\Delta S_m$, a smaller ΔS_m indicates a higher T_m. Therefore, the decrease in ΔS_m as a result of the chain confinement appears to be due to the higher melting endotherms. The reason why there are higher melting endotherms can be explained by the thermodynamic consideration, in which T_m is related to

$$T_m = \ell_c \Delta H_m \Delta T / 2\gamma\sigma_e$$

where ℓ_c is the lamellar thickness, ΔT, the degree of supercooling, γ, a constant and σ_e is the surface free energy of folding. As shown in Fig. 6, the long period, L is not a function of the blend compositions. Therefore, the higher melting endotherms suggest a strong influence of the restricted chain conformation on σ_e.

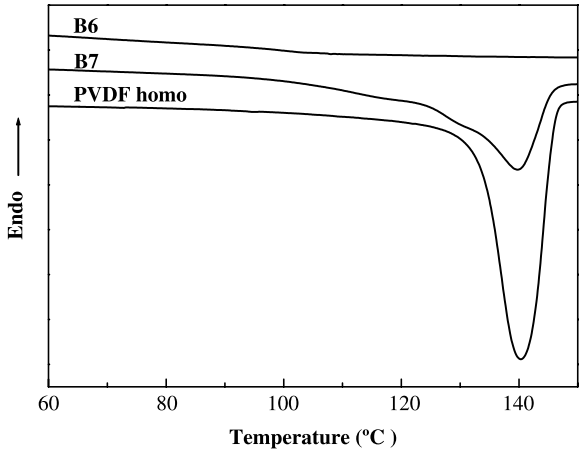

Fig. 9. Crystallization exotherms of the homo-PVDF and PVDF/PS-*b*-PMMA blends. The cooling rate was −10 °C/min.

The crystallization behavior of the blends is dependent on the ability of the component to crystallize. For example, the crystallization behavior characteristic of a single mode is expected if PVDF is mixed uniformly with the PMMA block segments, i.e. all the PVDF molecules have the same status. However, multimode crystallization will appear if some PVDF molecules have a different state. Fig. 9 shows the DSC cooling thermograms of the homo PVDF and its blends from the melt. For the B1 to B6 blends, the crystallization rate is too slow to detect exothermic pecks by DSC. Only one exotherm can be observed for homo-PVDF, whereas two exothermic peaks can be identified with a smaller exotherm developed at ca. 130 °C for the sample B7. For the B7 blend, some PVDF coexists with the PMMA segments, but some PVDF is restricted to form a PVDF core. It is likely that the two different PVDF portions will show a different crystallization behavior, resulting in the observation of two crystallization exotherms. The position of the first exothermic peak is similar to that of the crystallization peak for homo-PVDF. Therefore, the first exotherm might be due to the crystallization of the core PVDF, and the second exotherm might be associated with the crystallization of the PVDF mixed with PMMA-segments.

4. Conclusion

This study examined the morphological changes and crystallization behavior in various PVDF/PS-*b*-PMMA blends. At a low PVDF concentration, the PVDF was completely miscible with the PMMA microdomains. With increasing PVDF content, some PVDF was confined to a small area in the middle of the PMMA phase, leading to the formation of a PVDF core. Additional PVDF changed the morphology from a PMMA-cylindrical structure to a lamellar and finally a PS-cylindrical structure. The crystallization of PVDF caused a rearrangement and/or disturbance of the microdomain structures, resulting in a decrease in the structural order of the blends. PVDF exhibited a unique crystallization behavior depending on its miscibility in the PMMA block and space constraint. The crystallization of the core PVDF was similar to that of homo-PVDF, whereas the crystallization of the PVDF coexisting with the PMMA-segments was largely restricted.

Acknowledgements

This research was supported by the Korea Research Foundation (KRF-2004-041-D00202). Synchrotron SAXS experiments were performed at the Pohang Light Source (4C1 beam line) in Korea.

References

[1] Hashimoto T, Tanaka H, Hasegawa H. Macromolecules 1990;23:4378.
[2] Tanaka H, Hasegawa H, Hashimoto T. Macromolecules 1991;24:240.
[3] Winey KI, Thomas EL, Fetters LJ. Macromolecules 1991;24:6182.
[4] Roe RJ, Zin WC. Macromolecules 1984;17:189.

[5] Prahsarn C, Jamieson AM. Polymer 1997;38:1273.
[6] Meier DJ. Polym Prepr (Am Chem Soc Div Polym Chem) 1977;18:340.
[7] Liu LZ, Yeh F, Chu B. Macromolecules 1996;29:5336.
[8] Liu LZ, Li H, Jiang B, Zhou E. Polymer 1994;35:5511.
[9] Lee HK, Kang CK, Zin WC. Polymer 1996;37:287.
[10] Liu LZ, Chu B. J Polym Sci, Part B: Polym Phys 1999;37:779.
[11] Sakurai K, Macknight WJ, Lohse DJ, Schuiz DN, Sissano JA, Lin JS, et al. Polymer 1996;37:4443.
[12] Sakurai K, Macknight WJ, Lohse DJ, Schulz DN, Sissano JA. Macromolecules 1994;27:4941.
[13] Sakurai K, Macknight WJ, Lohse DJ, Schulz DN, Sissano JA. Macromolecules 1993;26:3236.
[14] Zhu L, Mimnaugh BR, Ge Q, Quirk RP, Cheng SZD, Thomas EL, et al. Polymer 2001;42:9121.
[15] Rangarajan P, Haisch CF, Register RA, Adamson DH, Fetters LJ. Macromolecules 1997;30:494.
[16] Buzarovska A, Koseva S, Cvetkovska M, Nedkov E. Eur Polym J 2001; 37:141.
[17] Radonjic G, Smit I. J Polym Sci, Part B: Polym Phys 2001;39:566.
[18] Lee W, Chen HL, Lin TL. J Polym Sci, Part B: Polym Phys 2002;40:519.
[19] Lowenhaupt B, Hellmann GP. Polymer 1991;32:1065.
[20] Hashimoto T, Kimishima K, Hasegawa H. Macromolecules 1991;24: 5704.
[21] Lu X, Weiss RA. Macromolecules 1993;26:3615.
[22] Luyten MC, Bogels EJF, Alberba van Ekenstein GOR, ten Brinke G, Bras W, Komanschek BE, et al. Polymer 1997;38:509.
[23] Kim JK, Jung DS, Kim JH. Polymer 1993;34:4613.
[24] Zhao H, Liu L, Tang T, Huang B. Polymer J 1998;30:775.
[25] Lee HK, Kang CK, Zin WC. Polymer 1997;38:1595.
[26] Sasaki H, Bala PK, Yoshida H, Ito E. Polymer 1995;36:4805.
[27] Linares A, Acosta JL. Eur Polym J 1997;33:467.
[28] Linares A, Acosta JL. J Appl Polym Sci 1998;67:997.
[29] Jeong U, Ryu DY, Kim JK, Kim DH, Russell TP, Hawker CJ. Adv Mater 2003;15:1247.
[30] Jeong U, Ryu DY, Kim JK, Kim DH, Wu X, Russell TP. Macromolecules 2003;36:10126.
[31] Jeong U, Ryu DY, Kho DH, Kim JK, Goldbach JT, Kim DH, et al. Adv Mater 2004;16:533.
[32] Jo SM, Lee WS, Ahn BS, Park KY, Paeng KA, Rhee IS. Polym Bull 2000;44:1.
[33] Bolze J, Kim JH, Huang JY, Rah SY, Youn HS. Macromol Res 2002;10:2.
[34] Hamley IW. The physics of block copolymers. New York: Oxford Science Publications; 1998.
[35] Cohen RE, Bellare A, Drzewinski MA. Macromolecules 1994;27:2321.
[36] Kofinas P, Cohen RE. Macromolecules 1994;27:3002.
[37] Liu L, Chu B. J Polym Sci, Part B: Polym Phys 1999;37:3819.
[38] Hamley IW, Fairclough JPA, Terril NJ, Ryan AJ, Lipic PM, Bates FS, et al. Macromolecules 1996;29:8835.
[39] Hamley IW, Fairclough JPA, Ryan AJ, Bates FS, Town-Andrews E. Polymer 1996;37:4425.
[40] Zhu L, Cheng SZD, Calhoun BH, Ge Q, Quirk RP, Thomas EL, et al. J Am Chem Soc 2000;122:5957.
[41] Quiram DJ, Register RA, Marchand GR, Adamson DH. Macromolecules 1998;31:4891.
[42] Loo YL, Register RA, Adamson DH. Macromolecules 2000;33:8361.
[43] Park C, Rosa CD, Fetters LJ, Thomas EL. Macromolecules 2000;33: 7931.
[44] Chen HL, Hasiao SC, Lin TL, Yamauchi K, Hasegawa H, Hashimoto T. Macromolecules 2001;34:671.
[45] Chen HL, Wu JC, Lin TL, Lin JS. Macromolecules 2001;34:6936.
[46] Lando JB, Olf HG, Peterlin A. J Polym Sci, A-1 1966;4:941.